Title
Visualization of ex vivo rabbit olfactory mucosa and foramina with three-dimensional optical coherence tomography

Journal
Lasers in Medical Science, 37(8)

ISSN
0268-8921

Authors
Pham, Tiffany Thienthao
Heidari, Andrew Emon
Hakimi, Amir Aaron
et al.

Publication Date
2022-10-01

DOI
10.1007/s10103-022-03598-w

Lasers in Medical Science (2022) 37:3203–3211
https://doi.org/10.1007/s10103-022-03598-w

ORIGINAL ARTICLE

Visualization of ex vivo rabbit olfactory mucosa and foramina with three-dimensional optical coherence tomography

Tiffany Thienthao Pham[1] · Andrew Emon Heidari[1,2] · Amir Aaron Hakimi[1] · Yan Li[1,2] · Cameron Michael Heilbronn[1,3] · Ellen Minyoung Hong[1] · Ji-Hun Mo[4,5] · Edward Cheng-Lung Kuan[3] · Zhongping Chen[1,2] · Brian Jet-Fei Wong[1,2,3]

Received: 23 October 2021 / Accepted: 19 June 2022 / Published online: 2 July 2022

Abstract

There is increasing interest in developing a minimally invasive imaging modality to safely evaluate dynamic microscopic changes of the olfactory mucosa and cribriform foramina. Herein, we utilized three-dimensional (3D) optical coherence tomography (OCT) to characterize the ex vivo stratified substructure of olfactory mucosa in rabbits and create 3D reconstructed images of olfactory foramina. Olfactory mucosa and cribriform plates from four New Zealand White rabbits were dissected and imaged using two swept-source OCT systems: (1) 1.3-μm (μm) center wavelength, 100-nm bandwidth, 200-kHz sweep rate, and (2) 1.7-μm center wavelength, 120-nm bandwidth, 90-kHz sweep rate. Volumetric OCT images were compiled to create a 3D reconstruction of the cribriform plate. The ability of OCT to distinguish the olfactory mucosa substructure and foramina was compared to histology. To estimate imaging penetration depth of each system, the first-order exponential decays of depth-resolved intensity were calculated and compared using a paired *t*-test. Three-dimensional OCT depicted the stratified layered structures within the olfactory mucosa correlating with histology. The epithelium and lamina propria were measured to be 32 μm and 107 μm in 1.3-μm OCT compared to 30 μm and 105 μm in histology. Olfactory foramina were visualized via 3D reconstruction. The 1.7-μm system provided greater depth penetration compared to the 1.3-μm system, allowing for improved foramina visualization. We have shown that OCT can be used to image non-pathologic olfactory mucosa and foramina. Implications for this work include diagnostic and therapeutic potentials for neurorhinological and neurodegenerative diseases.

Keywords Optical coherence tomography · Olfactory mucosa · Anterior skull base · Olfactory cleft · Olfactory foramina · Cribriform plate

Introduction

The mucosa of the posterosuperior nasal cavity contains olfactory neurons, which are the body's only surface neural cells and referred to by some as the "window to the brain" [1]. Olfactory neurons are ciliated bipolar neurons with axons that traverse the cribriform plate to enter the brain and synapse upon olfactory nerves. There has been longstanding interest in using olfactory epithelium (OE) biopsy for antemortem diagnostic testing of neurological disorders [2]. Olfactory dysfunction significantly impairs patient quality of life and is among the first clinical signs of neurologic and neurodegenerative disorders, which can present as hyposmia (and, in turn, dysgeusia) [3, 4]. Specifically, it is present in up to 100% with Alzheimer's disease (AD) and 90% with Parkinson's disease (PD) patients [5–7].

✉ Brian Jet-Fei Wong
bjwong@uci.edu

1 Beckman Laser Institute & Medical Clinic, University of California – Irvine, Irvine, CA, USA

2 Department of Biomedical Engineering, University of California - Irvine, Irvine, CA, USA

3 Department of Otolaryngology - Head and Neck Surgery, University of California - Irvine, School of Medicine, Orange, CA, USA

4 Beckman Laser Institute - Korea, Dankook University, Cheonan, Chungnam, Republic of Korea

5 Department of Otorhinolaryngology-Head and Neck Surgery, Dankook University, Cheonan, Chungnam, Republic of Korea

Although dystrophic neurites detected in postmortem OE of AD patients were initially thought to contribute to olfactory dysfunction, contemporary investigations have identified them in patients with other neurodegenerative disorders, and young and elderly controls without neurological disease [8–10].

Difficulties in interpreting OE may be due to intrinsic human OE irregularities, including patches of respiratory epithelium with non-uniform boundaries [11–13]. Various degrees of epithelial disorganization, degeneration, and respiratory metaplasia that can occur with increasing age can make histopathologic evaluation challenging [12]. Previous studies, however, did not evaluate longitudinal changes in vivo or possible neuronal bundle changes in the lamina propria (LP) which provide pathological information for other conditions of olfactory dysfunction [11]. Furthermore, invasive biopsy to sample tissue in this area poses a potential risk, as injury to the OE may lead to loss of smell or cerebrospinal fluid (CSF) leak, which may necessitate surgical repair. Thus, there is a need for a minimally invasive imaging tool to safely carry out such diagnostic evaluations.

Optical coherence tomography (OCT) is a near infrared, non-contact mesoscopic imaging modality that acquires depth-resolved information of tissues at micron-scale resolution [14]. OCT may be utilized to evaluate microscopic changes of the olfactory mucosa unresolved by traditional imaging modalities (e.g., CT, MRI) and may also be used to target or guide olfactory mucosa tissue biopsy. Promising studies have also shown that the olfactory mucosa is a source of olfactory ensheathing cells (specialized glia in the olfactory system) and multipotent neural stem cells, which may have use in autologous transplantation therapies to treat degenerative or traumatic disorders of the central nervous system, including spinal cord injury, stroke, or PD [15–18]. Fine-tuning the sampling process to one with safe and reliable means, while preserving olfaction and preventing CSF leak, is critical in this aspect and has been of great interest to scientists, neurologists, neurosurgeons, and otolaryngologists alike.

Herein, we demonstrate the feasibility of OCT to visualize the olfactory mucosa, to capture three-dimensional (3D) ex vivo images of the olfactory cleft and cribriform plate for foramina visualization in rabbits, and to correlate these images with histopathology. We hypothesize that 3D OCT can image the olfactory cleft and cribriform plate with associated foramina ex vivo.

Material and methods

This study was determined exempt from the University of California, Irvine Institutional Animal Care and Use Committee. Our experimental setup is depicted in Fig. 1. In this study, we dissected the nasal cavity and anterior skull base of four rabbits. These dissected tissue samples were imaged using two OCT systems with either a 1.3-μm (μm) or 1.7-μm

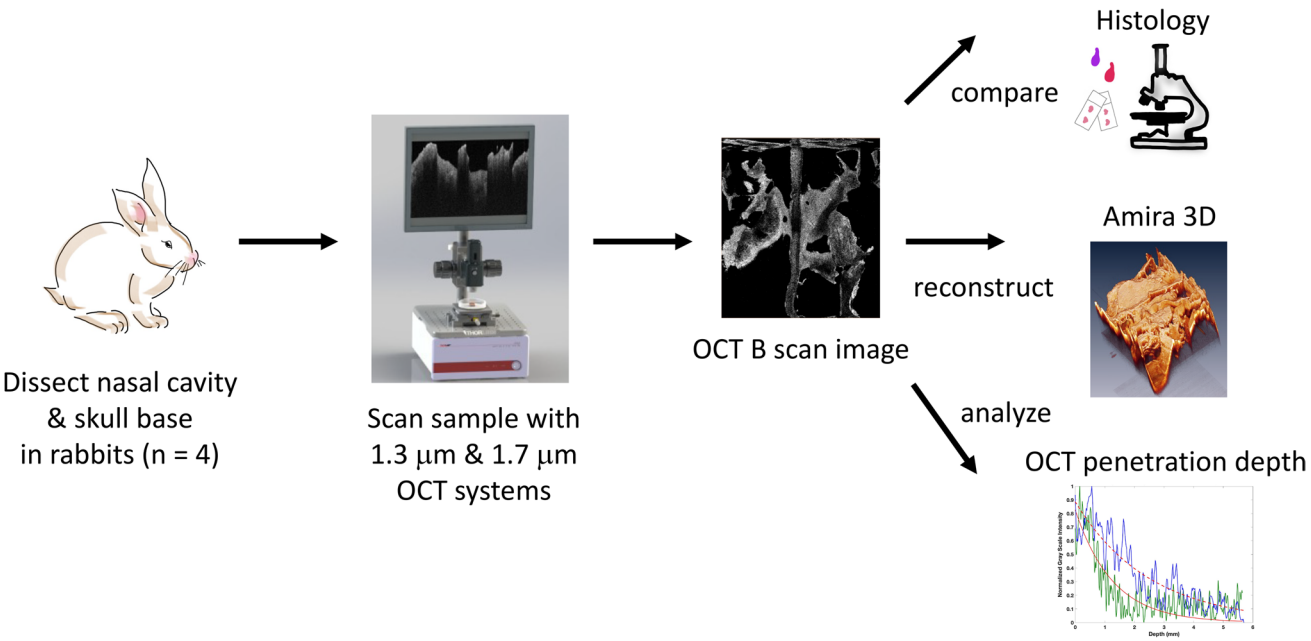

Fig. 1 Experimental setup. Four rabbits were dissected to attain the nasal cavity and skull base. The dissected tissue samples were then scanned using two OCT systems, with either a 1.3-μm or 1.7-μm center wavelength laser. The OCT B scan images were compared with histology slides from the tissue samples, reconstructed in 3D for morphology assessment, and analyzed to compare OCT penetration depths between the 1.3-μm or 1.7-μm OCT systems

center wavelength laser. The OCT images were compared with histology and reconstructed in 3D to assess morphology. We then compared the OCT penetration depth in the images attained by the 1.3-μm and 1.7-μm OCT systems.

Animal dissection

Four New Zealand White rabbits (*Oryctolagus cuniculus*), weighing approximately 4.0 kg, were obtained following euthanasia with 1.0 cc Euthasol (390 mg pentobarbital sodium, 50 mg phenytoin sodium, Vibrac AH, Inc. Fort Worth, TX, USA) administered through the marginal ear vein. The nasal cavity and anterior skull base of the New Zealand White rabbits were dissected anteriorly to posteriorly, according to previously described procedures [19]. The olfactory mucosa lining the posterosuperior nasal cavity in the olfactory cleft was identified using an atlas as an anatomic guide [19] and subsequently imaged from the ventral view, using two OCT microscope systems described below. The cribriform plate was dissected with the olfactory cleft and was imaged from the dorsal view.

OCT microscope systems and data acquisition

Two swept-source OCT microscope systems centered at 1.3 μm (1310 nm) and 1.7 μm (1710 nm) were used to image the dissected olfactory mucosa and cribriform plate in this study. The 1.3 μm OCT microscope system consisted of a commercial integrated Thorlabs OCT imaging system, two-dimensional galvanic imaging scanner, and vertical cavity surface emitting laser (VCSEL) (VEG220c1, Thorlabs, Thorlabs, Inc., Newton, NJ, USA). The 1.3 μm VCSEL laser was a 200 kHz, 1.3 μm center wavelength, swept-source VCSEL laser with a full-width half max bandwidth of 100 nm and axial resolution of 8 μm. The 1.3 μm center wavelength VCSEL was used in combination with the off-the shelf Thorlabs fiber-based Michelson interferometer (VEG220C1, Thorlabs). The sample arm of the Michelson interferometer was comprised of a 2D galvanic scanning microscope with an added scan lens (LSM03, Thorlabs) yielding a 12 μm lateral resolution. Using a scanning speed of 200 Hz, 1,000 OCT B-scan images of OCT data were acquired in 5 s over a 3D volume. A visible red light (HLS635, Thorlabs) coaxial to the laser beam indicated the scanned area. Visible light videos and images were concurrently recorded and used to co-register OCT data to correct scanning areas of the nasal cavity samples. OCT volumetric data were evaluated using FIJI software (ImageJ, National Institutes of Health, Bethesda, MD, USA) [20] and rendered into 3D representations of the olfactory cleft and cribriform plate using Amira software (Thermo Fisher Scientific, Waltham, MA, USA).

A custom 1.7 μm (1720 nm) OCT microscope system utilized a 90 kHz, 1.7 μm (1720 nm) center wavelength swept-source laser, with a bandwidth of 120 nm (HSL-40–90-B, Santec, Santec USA Corporation, Hackensack, NJ, USA), to image the olfactory mucosa and cribriform plate at greater penetration depths. The sample arm is comprised of a two-dimensional (2D) galvanic scanning system microscope: collimator (TC06APC-1550, Thorlabs), two-axis galvanometer mirrors (GVS102, Thorlabs), scan lens (LSM04, Thorlabs), and mount adapter (GCM102, Thorlabs). The reference arm is comprised of a collimator (TC06APC-1550, Thorlabs), lens (AC254-030-C, Thorlabs), mirror (PF10-03-M01, Thorlabs), and stage (PT1, Thorlabs). Axial and lateral resolutions are 17 μm and 25 μm, respectively. Using a scanning speed of 90 Hz, 1,000 OCT B-scan images of OCT data were acquired in 11 s over a 3D volume. Similarly, a visible red light, videos, and images were used for co-registration of OCT data to the scanned area.

OCT intensity–based penetration decay

Signal intensity penetration depth between 1.3 μm and 1.7 μm center wavelength OCT was compared to determine the optimal OCT system to image olfactory mucosa. Following scanning, the OCT volumes were re-sliced using FIJI software in the XY or enface direction to co-register the selected area for analysis using macroscopic features. Six corresponding A-lines were selected for both 1.7 μm and 1.3 μm OCT B-scans from the selected 2D OCT cross-section. The depth-resolved intensity data was then fit with a first-order exponential decay in MATLAB (v. 2018b, MathWorks, Natick, MA, USA) for each A-line to quantitatively assess variability in the decay constant. A larger exponential decay value correlated to faster intensity signal roll off and decreased signal depth penetration.

Statistical analysis

Using Microsoft Excel (v16.57, Microsoft, Redmond, WA, USA), a paired two-tailed *t*-test was utilized to compare the exponential decay values between the 1.7 μm and 1.3 μm OCT systems. Statistical significance was set at p-value ≤ 0.05, with alpha set at 0.05. An adequate sample size was determined with power at 0.80 and beta at 0.20.

Fixation and histology

Upon completion of imaging a given sample, the sample was then fully immersed in 10% formalin solution (SF1004, Fisher Chemical, Fisher Scientific, Hampton, NH, USA) and fixed for a minimum of 2 weeks prior to placement in a decalcifying solution (RDO-Gold Decalcifier, Electron Microscopy Sciences, Hatfield, PA, USA), continual

fixation, and routine processing [21]. Specimens were sectioned onto slides (AHS90-WH, Hareta, Springside Scientific, LLC., Durham, NC, USA) and stained with hematoxylin (MFCD00078111, Epredia, Kalamazoo, MI, USA) and eosin (MFCD00005040, Epredia) solution (H&E) which has been commonly used to study olfactory epithelium [22, 23]. H&E-stained histology slides were correlated with previously acquired OCT images by comparing similar features noted in OCT and histology, based on known resolution and scale.

Results

Histology of the olfactory mucosa on the cartilaginous septum showed OE, consisting of olfactory receptor neuron cell bodies and their cilia, supporting cells with microvilli, and basal cells (Fig. 2a). Bowman's glands were present in the LP that extend into the epithelium. Fine axon bundles from the olfactory neurons were also seen in the LP. Figure 2b depicts the correlative OCT B-scan of olfactory mucosa on the septum. The OE, LP, and septum were clearly delineated. The OE and LP were measured to be 32 µm and 107 µm, respectively, in 1.3-µm OCT, compared to 30 µm and 105 µm in histology, at the delineated green and yellow lines in Fig. 2a, b, suggesting correlation. At this resolution, individual neurons were not visualized in OCT, the spatial scattering signals within the LP vary laterally, suggesting possible topographical differentiation between the neuronal bundles and surrounding structures.

Visible light images of the dorsal and ventral aspects of the cribriform plate are seen in Fig. 3, with their corresponding OCT 3D reconstructions. The area that was scanned for each specimen is indicated by the dashed box (Fig. 3a–c). Grossly, olfactory mucosa was well-differentiated in the nasal cavity with a yellow-white hue, compared to the pink color of surrounding mucosa. Correlative morphology, including crista galli and olfactory foramina, is well visualized from the dorsal aspect. The ventral aspect of the cribriform plate depicts the olfactory cleft with the cartilaginous and bony septum and turbinates. Due to limitations in OCT signal depth of penetration, foramina visualized here (Fig. 3f) are likely within the nasal cavity and do not represent olfactory foramina.

Following further dissection posterosuperiorly within the nasal cavity to increase proximity to the cribriform plate, the ventral aspect of the cribriform plate was scanned with OCT and reconstructed (Fig. 4). These features were further investigated in FIJI shown in Fig. 4d–e in the enface XY and XZ perspective, respectively. Corresponding histology seen in Fig. 4f shows morphologic agreement with the XZ OCT B-scan in Fig. 4e and with the foramina present on the superior aspect of the cribriform plates seen as discontinuities within the cribriform plate bone, likely olfactory foramina.

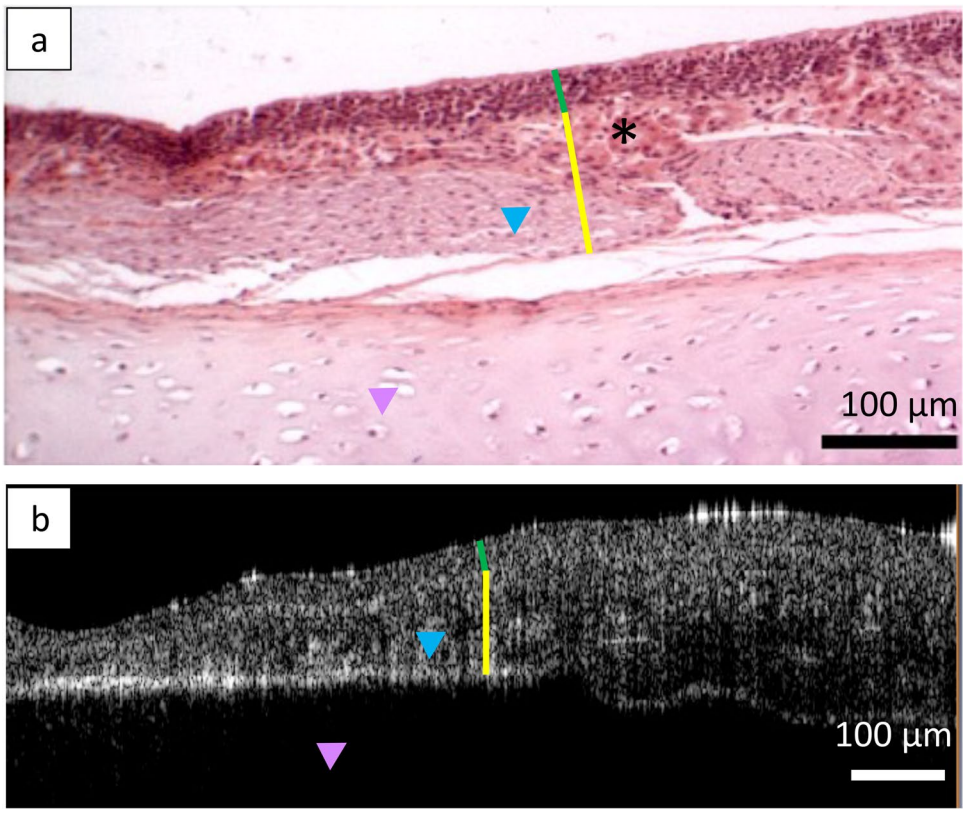

Fig. 2 OCT image of olfactory epithelium compared with histology. Coronal sections of (**a**) H&E histology and (**b**) OCT images. Green line: olfactory epithelium; yellow line: lamina propria; blue triangle: olfactory nerve bundles; black asterisk: Bowman's gland; pink triangle: cartilage

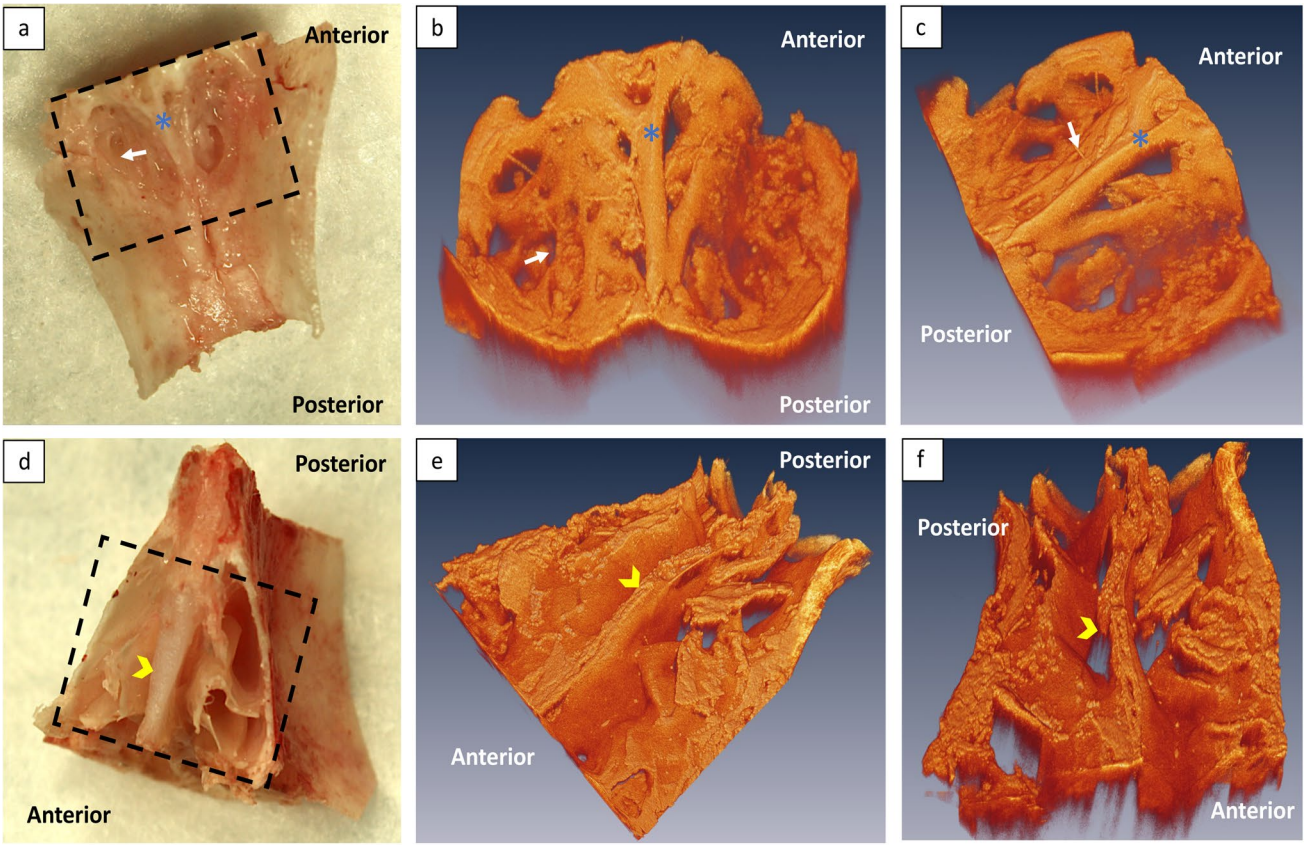

Fig. 3 3D reconstruction of cribriform plate and olfactory cleft. Visible light photographs: (**a**) dorsal cribriform plate, (**d**) ventral olfactory cleft; corresponding 3D reconstruction from OCT data: (**b**, **c**) dorsal aspect and (**d**, **e**) ventral aspect. Box: OCT scanned area; white arrow: foramina; blue asterisk: crista galli; yellow arrowhead: septum

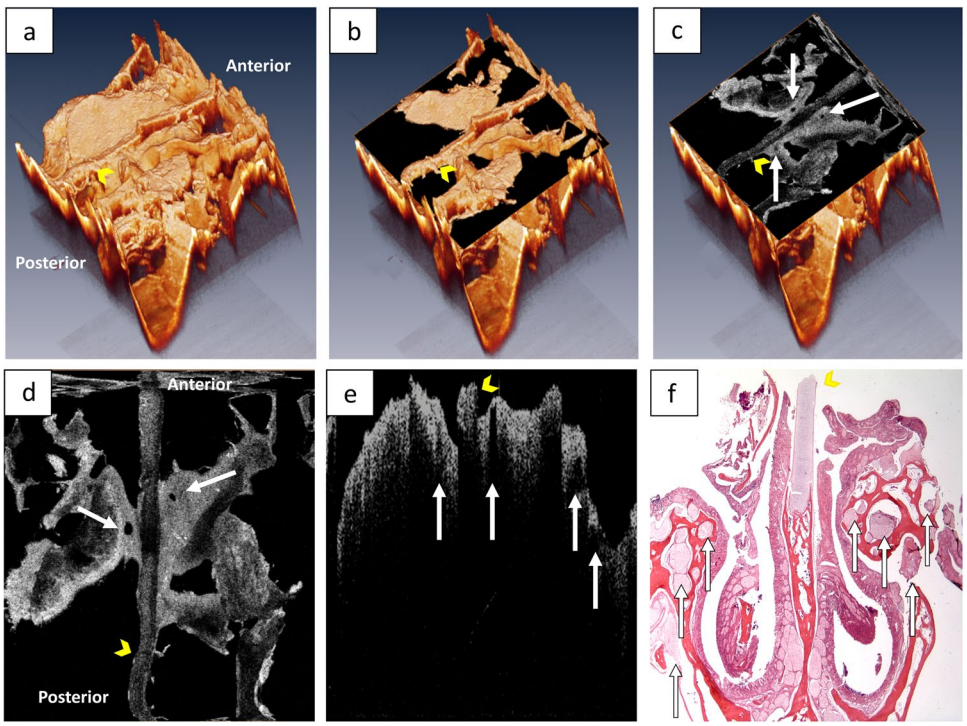

Fig. 4 3D reconstruction of olfactory cleft with demonstration of olfactory foramina. (**a**) 3D reconstruction of scanned OCT data showing ventral olfactory cleft; (**b**) transverse plane OCT section; (**c**, **d**) OCT sections demonstrating olfactory foramina; (**e**) coronal plane OCT section; (**f**) corresponding histological coronal sections demonstrating bone discontinuity, representing foramina. Yellow arrowhead: septum; white arrow: olfactory foramina

A comparison between 1.3 µm and 1.7 µm center wavelength SS-OCT depth penetration in the ventral aspect of olfactory cleft to the cribriform plate was performed (Fig. 5). In Fig. 5a–b, the enface OCT volume reconstruction is superimposed with a yellow line indicating a 2D OCT cross-section, representing the same scanned area shown in Fig. 5c–d for the 1.3 µm and 1.7 µm systems, respectively. Furthermore, a vertical corresponding A-line (indicated in green and blue color codes) within the OCT image was selected for OCT depth penetration analysis (Fig. 5e). Intensity plots for 1.3 µm and 1.7 µm, with corresponding mean first-order exponential decays, are shown. The mean first-order exponential decay for 1.3 µm was found to be greater than 1.7 µm [$-0.8062 \pm$ standard deviation (SD) 0.1735 versus -0.3855 ± 0.05872, respectively ($p < 0.001$)], indicating that the 1.3-µm depth-resolved intensity decays at a faster rate than the 1.7 µm. Depth penetration was greater for the 1.7-µm OCT system, with a slower signal decay.

Discussion

Whereas age-associated olfactory loss is normal, pathology of the OE, such as neurodegenerative-related deterioration, viral-induced olfactory loss, or idiopathic olfactory dysfunction can considerably impair patients' quality of life [24–26]. However, accurate monitoring of epithelial degeneration is limited by imaging modalities that lack adequate resolution to visualize structural topology, tissue structure, or cellular geometry. Additionally, diseases which produce localized mucosal or nerve injury cannot be reliably sampled due to significant associated risks. OCT has the potential to safely address some of these shortcomings, permitting mesoscopic imaging of biologic tissue with stratified structure [27].

Clinically, OCT has been primarily used to examine the retina, skin, and mucous membranes [28, 29]. Our group first introduced the potential for OCT to produce high-resolution images of the nasal mucosa [30]. In this study, we expand on this practice by utilizing 3D OCT to visualize the microstructure of the olfactory mucosa in the olfactory cleft and foramina within the cribriform plate in a rabbit model. OCT has the potential, at the very least, to provide information on this often difficult-to-access epithelium in a non-invasive fashion, which, like the skin, undergoes structural changes with age. Currently, the only modalities of evaluating the OE and cribriform plate are direct inspection using nasal endoscopy (often shielded by a septal swell body and/or middle turbinate), imaging (CT and/or MRI), or biopsy, which has an elevated risk of CSF leak and may disrupt residual olfaction. As such, the development of a means to perform an "optical biopsy" per se in a minimally invasive manner may

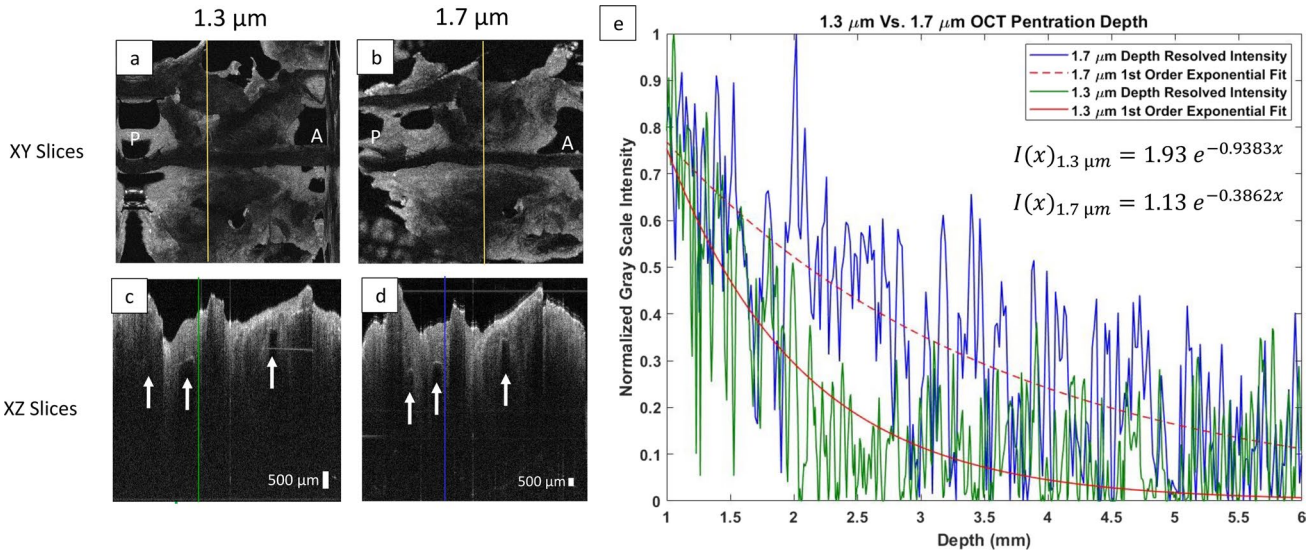

Fig. 5 Comparison of penetration depth between the 1.3 µm and 1.7 µm OCT systems. Enface ventral olfactory cleft with OCT 3D volume taken with (**a**) 1.3 µm and (**b**) 1.7 µm SS-OCT, with corresponding single OCT B-scan (**c**, **d**) respectively, taken at the yellow line superimposed on the paired XY scan. (**e**) Depth-resolved gray-scale intensity plots of two co-registered A-lines from the corresponding 1.3 µm (green line) and 1.7 µm (blue line) SS-OCT systems. First-order exponential decays were utilized to determine OCT penetration depth and are plotted in the figure as red solid and dashed lines superimposed on the line plot. Mathematical equations depict the first-order exponential decays of the corresponding A-lines highlighting the smaller first-order decay term for 1.7-µm SS-OCT and deeper signal penetration, compared to that of 1.3-µm SS-OCT. This analysis was repeated for five other adjacent A-lines. The average $\pm$ SD first-order exponential decay for 1.3-µm SS-OCT (-0.8062 ± 0.1735) was found to be greater than 1.7-µm SS-OCT (-0.3855 ± 0.05872) ($p < 0.001$). A: anterior; P: posterior; white arrow: olfactory foramina

have a significant role in management of various skull base disorders.

In our study, 3D OCT visualized the olfactory mucosa and cribriform plate with associated foramina, via reconstruction serial OCT sections. The OE, LP, septum, and cribriform plate were identified and correlated with histology. Although individual neurons and other cellular components were not clearly visualized using 1.3 μm and 1.7 μm wavelength lasers, moderate differentiation of neuronal bundles and surrounding structures may be seen. A broadband laser source that would allow sufficient axial resolution combined with high numerical aperture optics may enable improved visualization of cellular constituents. However, use of a broader source limits penetration depth of light, potentially inhibiting cribriform plate and foramina visualization.

Like all imaging modalities, there is a tradeoff between depth penetration and resolution. A previous study on OCT visualization of the olfactory mucosa by Ueda et al. showed the feasibility of estimating OE thickness in mice; however, in that study, only 2D visualization of olfactory mucosa was attained at a depth penetration of 1–2 mm at most [31]. A greater depth penetration was visualized in our study with 1–2 mm for the 1.3 μm system and 2–3 mm from the 1.7 μm system. The sweep rates of the OCT systems used in our study are 6.25 and 5.63 times faster for the 1.3 μm system and 1.7 μm system, respectively, which allows for rapid volumetric imaging in future in vivo studies. We used a more relevant animal model via the use of a New Zealand White rabbit, which is larger than mice with greater osseous thickness and at least resembles human neonates. With visualization of the stratified structure, it may be possible to monitor changes to olfactory mucosal thickness, LP containing neuronal bundles, and macroscopic structures associated with various disease states. This may translate into clinical value in that no invasive sampling may be necessary to distinguish various pathologies or changes related to this sensitive area.

The ventral surface of the cribriform plate with olfactory foramina was well visualized through the posterosuperior nasal cavity in the olfactory cleft. Three-dimensional OCT permitted clear foramina visualization, which otherwise would not have been readily seen with 2D OCT images. There has been great interest in studying olfactory foramina and creating 3D reconstructed images of the cribriform plate using CT imaging [32–34]. This is the first study utilizing OCT imaging to demonstrate similar capabilities to CT, albeit in a rodent model. The advantages of OCT compared to CT or MRI imaging include its micron-scale resolution demonstrating morphology at both a cellular and structural level, speed and ease of use, and overall safety profile for in vivo imaging. Moreover, OCT presents image information in real-time and with appropriate graphic processing units could provide 3D images useful for navigation. Thus, it may serve as a valuable tool for image-guided therapy, possibly targeting the central nervous system (CNS) through olfactory foramina.

As another possible application, the ability to bypass the blood–brain barrier to deliver pharmaceutical therapies has been referred to as a "holy grail" of neuropharmacology [35]. Intranasal drug delivery has been of particular interest because it is the only site of the human body where the nervous system is in direct contact with its environment. Nevertheless, several factors can influence intranasal drug delivery including head position, drug administration technique, and drug formulation [36]. More recently, Miyake and Bleier proposed an endoscopic surgical technique for direct intranasal drug delivery to the CNS using heterotopic mucosal grafts [35]. However, this requires surgical intervention and its efficacy is subject to the post-transplant barrier and permeability characteristics of free mucosal grafts. Alternatively, our proposed technique could allow for micro-invasive access to intracranial tissues under direct OCT-based visualization of the foramina. Pre-operative 3D reconstructions of the area of interest can guide procedural planning. Theoretically, this could be done more quickly than endoscopic surgery and patients would be subjected to a shortened recovery time.

Our study also demonstrated the variability in depth penetration of two swept-source OCT systems of varying center wavelengths, namely, 1.3 μm and 1.7 μm. It has been previously indicated that 1.7 μm OCT has a greater penetration depth compared to 1.3 μm, and this was as expected [37–39]. Due to the light scattering relationship between the wavelength and particle size, 1.7 μm wavelength light scatters preferentially forward (rather than back or side scattered), permitting light diffusion deeper into the sample. Thus, laser light centered at 1.7 μm has a higher probability of propagating deeper through the thickness of the olfactory mucosa, as seen in this study. Deeper penetration into the tissues provided for better olfactory foramina visualization beyond the olfactory mucosa from the ventral aspect of the nasal cavity. Further development of low coherence sources and systems to include greater axial visualization of tissues would be useful. Enabling deep imaging at micron level resolution, OCT systems may potentially be utilized to evaluate the OE to assess for neurologic or neurorhinological disorders, and may help guide transnasal, intracranial interventions.

We acknowledge several limitations of our investigation. Since the tissues are highly responsive to the aqueous nature of their environment, specimen hydration may impact our findings. We attempted to control for this as much as possible by wrapping the specimens in HBSS soaked gauze immediately after dissection. Additionally, although we utilized microscope scanning OCT systems to visualize tissue microanatomy, the large form factor of the objective lenses with an outer diameter of 43 mm limits the use of such a system to ex vivo or in vitro

imaging. Miniaturization of OCT systems to endonasally image the olfactory mucosa and surrounding structures is a technical challenge that we are in the process of addressing, but have in the past built such systems and fiber endoscopic probes for other imaging applications [40–44]. With miniaturization of the probe, lateral resolution will be sacrificed. However, using a gradient refractive index relay rod to transmit the light, one may be capable of maintaining sufficient lateral resolution. Furthermore, utilizing a super continuum diode laser to improve axial resolution may provide better resolution to differentiate the olfactory anatomy. Nevertheless, in this preliminary study, we have shown the ability of 3D OCT to resolve the stratified structure of the olfactory mucosa and olfactory foramina within the olfactory cleft and cribriform plate in an ex vivo rabbit model. Future planned studies will include development of image processing algorithms to segment and differentiate the stratified structure in 2D and 3D volumes. Furthermore, we aim to translate this work into in vivo imaging and human subjects, starting with cadaver studies, with development of suitable endoscopic OCT devices.

Conclusion

OCT is a minimally invasive means of evaluating topographical differentiation of olfactory mucosa and surrounding structures. We observed distinctive olfactory mucosal structures and olfactory foramina in the OCT images that correlate with their respective histology. Potential implications include investigational and diagnostic purposes for neurologic and neurorhinological disorders, and image guidance for transnasal, intracranial interventions.

Acknowledgements We thank Jean Fang for her assistance with animal dissections.

Author contribution Conceptualization: Brian Jet-Fei Wong.

Methodology: Tiffany Thienthao Pham, Andrew Emon Heidari, Zhongping Chen, Brian Jet-Fei Wong.

Formal analysis: Tiffany Thienthao Pham, Andrew Emon Heidari, Amir Aaron Hakimi, Brian Jet-Fei Wong.

Investigation: Tiffany Thienthao Pham, Andrew Emon Heidari, Yan Li, Cameron Michael Heilbronn, Ellen Minyoung Hong.

Data Curation: Tiffany Thienthao Pham, Andrew Emon Heidari, Yan Li, Cameron Michael Heilbronn, Ellen Minyoung Hong.

Visualization: Tiffany Thienthao Pham, Andrew Emon Heidari.

Writing — original draft: Tiffany Thienthao Pham.

Writing — review and editing: Tiffany Thienthao Pham, Andrew Emon Heidari, Amir Aaron Hakimi, Yan Li, Cameron Michael Heilbronn, Ellen Minyoung Hong, Ji-Hun Mo, Edward Cheng-Lung Kuan, Zhongping Chen, Brian Jet-Fei Wong.

Project administration: Tiffany Thienthao Pham.

Funding acquisition: Ji-Hun Mo, Brian Jet-Fei Wong.

Resources: Zhongping Chen, Brian Jet-Fei Wong.

Funding This study was funded by the Irvine Head and Neck Research Foundation and the Leading Foreign Research Institute Recruitment Program through the National Research Foundation of Korea (NRF) funded by the Ministry of Science and ICT (MSIT) [2012K1A4A3053142].

Declarations

Ethical approval This study was given exemption status from the Institutional Review Board of the University of California – Irvine.

Informed consent No informed consent was necessary for this study.

Conflict of interest Zhongping Chen has financial interests in OCT Medical Imaging, Inc., which however, did not support this research.

References

1. Godoy MDCL, Voegels RL, Pinna FDR, Imamura R, Farfel JM (2015) Olfaction in neurologic and neurodegenerative diseases: a literature review. Int Arch Otorhinolaryngol 19:176–179
2. Lanza DC, Moran DT, Doty RL, Trojanowski JQ, Lee JH, Rowley JC, Crawford D, Kennedy DW (1993) Endoscopic human olfactory biopsy technique. Laryngoscope 103:815–819
3. Doty RL (2009) The olfactory system and its disorders. Semin Neurol 29:74–81
4. Joseph T, Auger SD, Peress L, Rack D, Cuzick J, Giovannoni G, Lees A, Schrag AE, Noyce AJ (2019) Screening performance of abbreviated versions of the UPSIT smell test. J Neurol 266:1897–1906
5. Doty RL (2012) Olfaction in Parkinson's disease and related disorders. Neurobiol Dis 46:527–552
6. Ross GW, Petrovitch H, Abbott RD, Tanner CM, Popper J, Masaki K, Launer L, White LR (2008) Association of olfactory dysfunction with risk for future Parkinson's disease. Ann Neurol 63:167–173
7. Zou YM, Lu D, Liu LP, Zhang HH, Zhou YY (2016) Olfactory dysfunction in Alzheimer's disease. Neuropsychiatr Dis Treat 12:869–875
8. Lee JH, Goedert M, Hill WD, Lee VM, Trojanowski JQ (1993) Tau proteins are abnormally expressed in olfactory epithelium of Alzheimer patients and developmentally regulated in human fetal spinal cord. Exp Neurol 121:93–105
9. Trojanowski JQ, Newman PD, Hill WD, Lee VM (1991) Human olfactory epithelium in normal aging, Alzheimer's disease, and other neurodegenerative disorders. J Comp Neurol 310:365–376
10. Crino PB, Greenberg B, Martin JA, Lee VM, Hill WD, Trojanowski JQ (1995) β-amyloid peptide and amyloid precursor proteins in olfactory mucosa of patients with Alzheimer's disease, Parkinson's disease, and Down syndrome. Ann Otol Rhinol Laryngol 104:655–661
11. Holbrook EH, Leopold DA, Schwob JE (2005) Abnormalities of axon growth in human olfactory mucosa. Laryngoscope 115:2144–2154
12. Paik SI, Lehman MN, Seiden AM, Duncan HJ, Smith DV (1992) Human olfactory biopsy: the influence of age and receptor distribution. Arch Otolaryngol Neck Surg 118:731–738
13. Lane AP, Gomez G, Dankulich T, Wang H, Bolger WE, Rawson NE (2002) The superior turbinate as a source of functional human olfactory receptor neurons. Laryngoscope 112:1183–1189

14. Huang D, Swanson EA, Lin CP, Schuman JS, Stinson WG, Chang W, Hee MR, Flotte T, Gregory K, Puliafito CA, Fujimoto JG (1991) Optical coherence tomography. Science 254:11783–21181
15. Chiu SC, Hung HS, Lin SZ, Chiang E, Liu DD (2009) Therapeutic potential of olfactory ensheathing cells in neurodegenerative diseases. J Mol Med 87:1179–1189
16. Mackay-Sim A, Féron F, Cochrane J, Bassingthwaighte L, Bayliss C, Davies W, Fronek P, Gray C, Kerr G, Licina P, Nowitzke A, Perry C, Silburn PAS, Urquhart S, Geraghty T (2008) Autologous olfactory ensheathing cell transplantation in human paraplegia: A 3-year clinical trial. Brain 131:2376–2386
17. Lima C, Pratas-Vital J, Escada P, Hasse-Ferreira A, Capucho C, Peduzzi JD (2006) Olfactory mucosa autografts in human spinal cord injury: a pilot clinical study. J Spinal Cord Med 29:191–203
18. Murrell W, Wetzig A, Donnellan M, Féron F, Burne T, Meedeniya A, Kesby J, Bianco J, Perry C, Silburn P, Mackay-Sim A (2008) Olfactory mucosa is a potential source for autologous stem cell therapy for Parkinson's disease. Stem Cells 26:2183–2192
19. Pereira ME, Macri NP, Creasy DM (2011) Evaluation of the rabbit nasal cavity in inhalation studies and a comparison with other common laboratory species and man. Toxicol Pathol 39:893–900
20. Schindelin J, Arganda-Carreras I, Frise E, Kaynig V, Longair M, Pietzsch T, Preibisch S, Rueden C, Saalfeld S, Schmid B, Tinevez JY, White DJ, Hartenstein V, Eliceiri K, Tomancak P, Cardona A (2012) Fiji: an open-source platform for biological-image analysis. Nat Methods 9:676–682
21. Rolls G (2011) Difficult blocks and reprocessing. Leica Microsyst 9:1–108
22. Camacho S, Ostos-Garrido MV, Domezain A, Carmona R (2010) Study of the olfactory epithelium in the developing sturgeon. Characterization of the crypt cells. Chem Senses 35:147–156
23. De Rezende PF, Ctenas B, Weber R, Saldiva PH, Voegels RL (2013) Olfactory neuroepithelium in the superior and middle turbinates: which is the optimal biopsy site? Int Arch Otorhinolaryngol 17:131–138
24. Graziadei PP, Graziadei GA (1979) Neurogenesis and neuron regeneration in the olfactory system of mammals. I. Morphological aspects of differentiation and structural organization of the olfactory sensory neurons. J Neurocytol 8:1–18
25. Boesveldt S, Postma EM, Boak D, Welge-Luessen A, Schöpf V, Mainland JD, Martens J, Ngai J, Duffy VB (2017) Anosmia-A clinical review. Chem Senses 42:513–523
26. Edge AS, Chen ZY (2008) Hair cell regeneration. Curr Opin Neurobiol 18:377–382
27. Drexler W, Fujimoto JG (2015) Optical coherence tomography: technology and applications, 2nd edn. Switzerland
28. Krauss JM, Puliafito CA (1995) Lasers in ophthalmology. Lasers Surg Med 17:102–159
29. Welzel J (2001) Optical coherence tomography in dermatology: a review. Ski Res Technol 7:1–9
30. Mahmood U, Ridgway J, Jackson R, Guo S, Su J, Armstrong W, Shibuya T, Crumley R, Chen Z, Wong B (2006) In vivo optical coherence tomography of the nasal mucosa. Am J Rhinol 20:155–159
31. Ueda T, Sakamoto T, Kobayashi M, Kuwata F, Ishikawa M, Omori K, Nakagawa T (2019) Optical coherence tomography for observation of the olfactory epithelium in mice. Auris Nasus Larynx 46:230–237
32. Girerd C, Lihoreau T, Rabenorosoa K, Tamadazte B, Benassarou M, Tavernier L, Pazart L, Haffen E, Andreff N, Renaud P (2018) In vivo inspection of the olfactory epithelium: feasibility of robotized optical biopsy. Ann Biomed Eng 46:1951–1961
33. Farneti P, Riboldi A, Sciarretta V, Piccin O, Tarchini P, Pasquini E (2017) Usefulness of three-dimensional computed tomographic anatomy in endoscopic frontal recess surgery. Surg Radiol Anat 39:161–168
34. Bird DJ, Amirkhanian A, Pang B, Van Valkenburgh B (2014) Quantifying the cribriform plate: influences of allometry, function, and phylogeny in carnivora. Anat Rec 297:2080–2092
35. Miyake MM, Bleier BS (2015) Bypassing the blood–brian barrier using established skull base reconstruction techniques. World J Otorhinolaryngol Neck Surg 1:11–16
36. Dhuria SV, Hanson LR, Frey WH (2010) Intranasal delivery to the central nervous system: mechanisms and experimental considerations. J Pharm Sci 99:1654–1673
37. Li Y, Jing J, Heidari E, Zhu J, Qu Y, Chen Z (2017) Intravascular optical coherence tomography for characterization of atherosclerosis with a 1.7 micron swept-source laser. Sci Rep 7:14525
38. Pham TT, Chen L, Heidari AE, Chen JJ, Zhukhovitskaya A, Li Y, Patel U, Chen Z, Wong BJF (2019) Computational analysis of six optical coherence tomography systems for vocal fold imaging: a comparison study. Lasers Surg Med. https://doi.org/10.1001/lsm.23060
39. Li Y, Sudol NT, Miao Y, Jing JC, Zhu J, Lane F, Chen Z (2019) 1.7 micron optical coherence tomography for vaginal tissue characterization in vivo. Lasers Surg Med 51:120–126
40. Lin JL, Yau AY, Boyd J, Hamamoto A, Su E, Tracey L, Heidari AE, Wang AH, Ahuja G, Chen Z, Wong BJ (2013) Real-time subglottic stenosis imaging using optical coherence tomography in the rabbit. JAMA Otolaryngol Head Neck Surg 139:502–509
41. Liu G, Rubinstein M, Saidi A, Qi W, Foulad A, Wong B, Chen Z (2011) Imaging vibrating vocal folds with a high speed 1050 nm swept source OCT and ODT. Opt Express 19:11880–11889
42. Tang S, Jung W, McCormick D, Xie T, Su J, Ahn Y-C, Tromberg BJ, Chen Z (2009) Design and implementation of fiber-based multiphoton endoscopy with microelectromechanical systems scanning. J Biomed Opt 14:034005
43. Jung W, Tang S, McCormic DT, Xie T, Ahn Y-C, Su J, Tomov IV, Krasieva TB, Tromberg BJ, Chen Z (2008) Miniaturized probe based on a microelectromechanical system mirror for multiphoton microscopy. Opt Lett 33:1324–1326
44. Miao Y, Brenner M, Chen Z (2019) Endoscopic optical coherence tomography for assessing inhalation airway injury: a technical review. Otolaryngol (Sunnyvale) 9:366